Fig. 18.1. Annual mean equilibrium surface temperature (°C) for the world ocean. This is the temperature the sea surface would have if the heat budget were locally balanced at all times. Note the similarity with the observed annual mean surface temperature (Fig. 2.5a) but also the differences in regions of strong currents and upwelling. From Hirst and Godfrey (1992).

A somewhat better approximation to this situation is to treat the ocean as a passive "slab", perhaps 100 m deep, i.e. to allow it to absorb heat during summer and release it again in winter, through the formation of the seasonal mixed layer (Chapter 5). Relative to the atmosphere, the storage capacity of the ocean for heat is huge (about 1000 kcal are released by every 3100 m^3 of dry air or 1 m^3 of sea water if their temperature is lowered by 1°C). This results in a seasonal SST cycle almost three months out of phase with the solar heating and much reduced in amplitude compared to that found in places far from the sea. Thus heat storage in the mixed layer results in milder climates for coastal and island locations, and a slab model can reproduce these effects quite well.

However, both the swamp and slab models are very deficient for representing the earth's mean climate, particularly if one wishes to understand its year-to-year variations. The ocean can and does absorb heat in one region, carry the heated water below the surface by subduction (Figure 5.3) or deep convection, and return the heat to the atmosphere many thousands of kilometers away and years, decades or even centuries later. In the mean, this results in the transport of heat from the equator towards the poles, tending to cool the tropics and heat the polar regions; the efficiency of this process is comparable to that of the atmosphere (Figure 18.2). The difference is that this process is carried out by ocean currents with a cycle time of many years. The strength of these currents varies, so we can expect year-to-year variations of the heat exchange with the atmosphere. To give two examples, the big region of heat gain in the eastern equatorial Pacific seen in Figure 1.6 largely disappears in some years (known as El Niño years, discussed in Chapter 19), with drastic effects on the world's climate; and there are reasons to suspect that the region of heat

devised for estimating the flux of solar radiation into the ocean from data on cloud cover, which have been collected by merchant ship's officers; world maps of solar (or "short-wave") radiation entering the ocean (such as Figure 1.5) are essentially maps of merchant ship cloud cover estimates, modulated by the geographic variation of clear-sky radiation (which is simply a function of latitude and season). Even with "perfect" cloud data, different algorithms (known as bulk formulae) differ in their estimates of the net solar radiation by about 10 - 20% (e.g. Hanawa and Kizu, 1990). Evaporation cools the ocean surface and is responsible for the second most important term in the heat budget, *latent heat loss* (Figure 18.3), particularly in the tropics. It can be estimated from other simple rules, using data on wind speed, the "wet bulb" and "dry bulb" temperatures, and sea surface temperature, all of which are also routinely collected by merchant ship officers. Again, different algorithms can yield results that differ by as much as 30 W m^{-2} (Godfrey *et al.*, 1991; 30 W m^{-2} is enough to warm a layer of water 50 m thick by 0.5°C per month).
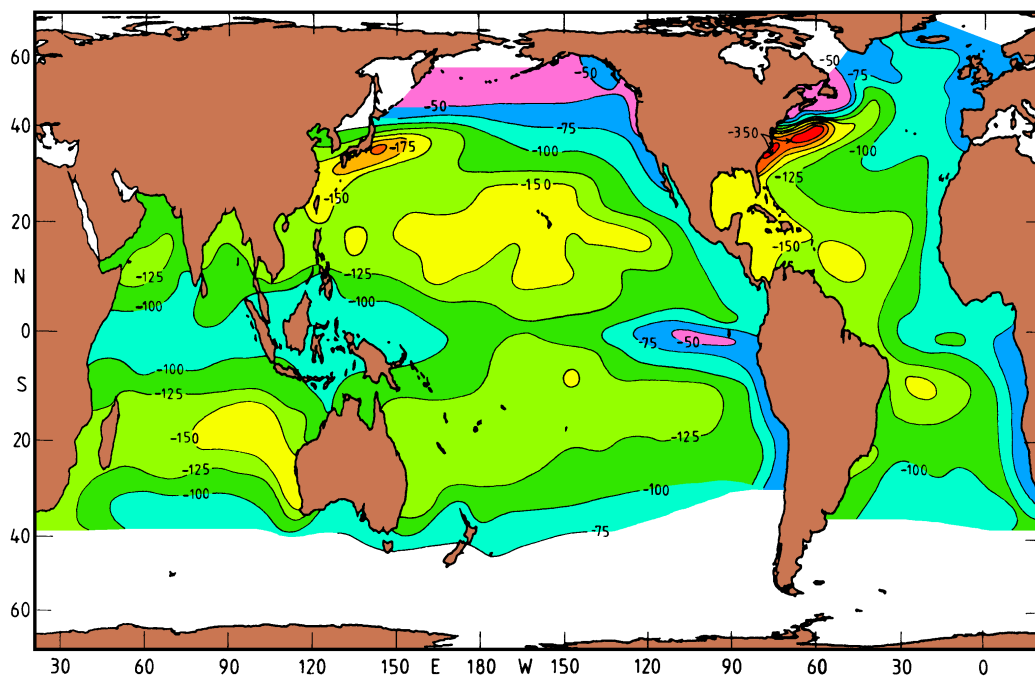

Fig. 18.3. Annual mean latent heat flux (W m^{-2}). Oceanic heat loss to the atmosphere is shown as negative numbers. From Oberhuber (1988).

Two other types of heat flux - *sensible heat transfer* (the direct, mechanical transfer of heat between air and water when the two media have different temperatures) and *net longwave radiation* (the net escape of thermal radiation from the ocean surface) - contribute to the total heat flux; they are generally smaller than the first two but not small enough to be neglected. These also can be estimated from simple rules, using the same merchant ship

Upwelling typically produces several degrees of cooling. The large net heat flux into the ocean in coastal upwelling regions is thus readily understood.

Coastal upwelling occurs only in the first few tens of kilometers from the coast, whereas the coastal bands of heat gain in Figure 1.6 are as much as a thousand kilometers or more in width, so coastal upwelling by itself does not explain the existence of these bands of heat flux into the ocean. However, the heat capacity of the surface mixed layer is so great that the upwelled water takes several months to warm to the equilibrium temperature; during these months the water can move 1000 km or so offshore with the Ekman drift. Furthermore, after the water is upwelled, it flows equatorward with the Sverdrup flow. Consequently the water moves into steadily warmer climates, causing it to continue to warm for substantial periods after it has upwelled. This advective contribution to surface heating is clearly seen by comparing the annual mean SST map (Figure 2.5a) with surface currents (Figures 8.6 and 14.2). In each of the eastern boundary upwelling regions, the surface currents clearly flow from low temperatures towards high.

Equatorial upwelling regions

Strong bands of oceanic heat gain along the equator are found over the entire width of the Atlantic and over the eastern Pacific Oceans; weaker heat gain occurs in the west Pacific Ocean. Comparison with Figure 1.4a shows that there are moderate easterly wind stresses along the equator in both oceans; in relative terms they are strongest on the western side of the Atlantic and in the central Pacific Ocean.

These winds give rise to large poleward Ekman transports on either side of the equator (Figure 4.1). Upwelling occurs to replace the water that is removed by Ekman transport, as discussed in Chapter 8. The upwelled water is in turn supplied by geostrophically balanced flow in the top few hundred meters. A zonal steric height gradient develops to keep these meridional flows in geostrophic balance. (The Coriolis force changes direction across the equator, so the same zonal steric height gradient produces meridional flows of opposite sign on either side of the equator.) This zonal steric height gradient can be seen along the equator in both the Pacific and Atlantic Oceans in Figure 2.8b.

The heat flux maximum in the equatorial Pacific and Atlantic Oceans (Figure 1.6) lies somewhat to the east of the strongest equatorial easterly winds (Figure 1.4a), i.e. to the east of the strongest upwelling. The reason is that the temperature of upwelled water decreases eastwards along the equator, being coldest at the east of each basin. This fact in turn relates to the zonal gradient of steric height along the equator, set up to balance the wind and provide geostrophic inflow. Since steric height is roughly speaking a vertical integral of temperature, the zonal steric height gradient forces near-surface temperatures to be colder at the eastern end of each basin, where the steric height is lower.

As in the case of the eastern boundary heating regions, the width of the equatorial heating region extends about 1000 km on either side of the equator, much wider than the region of actual upwelling. The reason is again the same as in the coastal upwelling regions. After the water upwells it takes several months for it to absorb enough heat to reach thermal equilibrium with the atmosphere, during which time it can travel 1000 km poleward with the Ekman drift.

Two other factors not related to upwelling also influence equatorial SST in the Pacific and Atlantic Oceans. Both are related to current shear. Vertical current shear between the westward surface flow and the eastward flowing Equatorial Undercurrent produces increased

else. In Chapter 13 it was argued that turbulent mixing must be anomalously strong in Indonesian waters and that its effect must be felt to 1000 m depth. This reduces SST and distributes the heat input from the atmosphere over a deeper "slab" then elsewhere in the world ocean. This is the only equatorial region in the world ocean were large heat gain is achieved without upwelling.

The Leeuwin Current

The zero heat flux contour in Figure 1.6 meets the continents near 50°N and S in the eastern Atlantic and Pacific Oceans but closer to 20°S in the Indian Ocean. This major difference between the ocean basins does not reflect a difference in the wind regime (Figure 1.4a) but a difference in the details of the eastern boundary regime. As discussed in Chapter 11, the upwelling that one might expect from the equatorward winds between 20° and 34°S along the western Australian coast is overwhelmed by an onshore geostrophic drift. The meridional pressure gradient needed to maintain the onshore drift is supplied by heat loss near Western Australia (clearly seen in Fig 1.6) which cools water at the southern end of the continent, reducing steric height from the very high levels found off northwestern Australia. This is one rare instance in which the currents carrying heat fluxes in the ocean are created by the heat fluxes themselves, i.e. by thermohaline processes; most surface currents are driven by wind forcing. However, as remarked in Chapter 11, the whole Leeuwin Current system can be regarded as being driven by winds along the equatorial Pacific Ocean, which pile up warm water in the west Pacific region and hence bring very warm water to northwestern Australia.

The subtropical western boundaries

One feature which emerges clearly from Figure 1.6 is that the Kuroshio and Gulf Stream and its extensions release massive amounts of heat to the atmosphere. This occurs mainly in winter when cold winds blow from Siberia and Canada respectively across the warm, poleward flowing waters of these currents; heat loss during summer is low and may turn into heat gain on occasions. On annual average, however, heat is lost from the ocean in the western boundary currents and extension regions. This heat loss results in convective sinking of surface water, so the extension regions of western boundary currents in the northern hemisphere are important regions for water mass formation. The subtropical mode waters have their origin in these regions, from where they are subducted into the subtropical gyres of the north Pacific and Atlantic Oceans.

By contrast, the heat losses from the western boundary currents of the Southern Hemisphere seem very small. In the case of the Brazil and East Australian Currents data are probably quite adequate to yield reasonable heat flux estimates, so that the small heat losses associated with these two currents are probably valid. Furthermore, the result is not unexpected. First, both currents are quite weak, the Brazil Current because it is opposed by the thermal flow towards the north Atlantic Ocean and the East Australian Current because a substantial fraction of its potential transport is drained away by the Indonesian throughflow. Secondly, no analogue of the very cold and dry Canadian and Siberian winter winds blow over either of these two currents.

The apparent weakness of the heat loss from the Agulhas Current and its extension suggested by Figure 1.6 is harder to understand and may be an artifact of the climatology.

Pacific from the Atlantic Ocean; yet it is low enough to permit moisture transport across it in the atmosphere, so that the north Atlantic Ocean becomes salty while the north Pacific Ocean becomes fresh. One may therefore say that northwestern Europe is warmer than Canada and Alaska because there is a low but complete land blockage in Central America.

The global freshwater and salt budgets

As noted earlier, estimates of precipitation and evaporation over the ocean (Figure 1.7) are subject to even greater uncertainties than the net heat flux field. Consequently we will not discuss the freshwater and salt budgets nearly as fully as the heat budget. We begin by noting two things. Firstly, it is evident from our earlier considerations on the transport of heat at the end of Chapter 4 that a net transport of salt or of freshwater can exist even if the net mass transport is zero. Secondly, salt and freshwater can both be transported in the same direction. This fact is somewhat contrary to intuition, since one might think that relative to the oceanic mean, freshwater is negative salt load and should therefore always be flowing in a direction opposite to the direction of the salt flux (readers familiar with estuarine oceanography will recognize this concept). Figure 18.4 shows that this is not so when the P - E difference becomes a major contribution to the budget. The two quantities are then no longer inversely related.
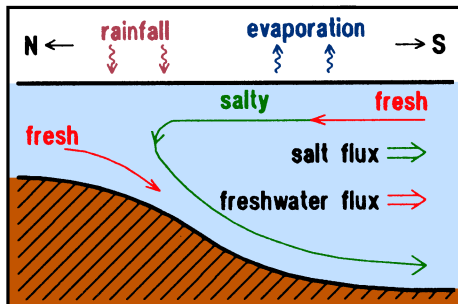

Fig. 18.4. A sketch of salt and freshwater transport in an ocean basin resembling the north Atlantic Ocean. At the surface, water gets saltier as it moves from the tropics through the subpolar gyre to the region where it sinks to carry salt southward in the deeper layers; this produces southward salt transport. Freshwater is imported from the Arctic Mediterranean Sea, in quantities not sufficient to lower the salinity in the deeper layer beyond the tropical surface salinities; while it therefore does not reverse the salt flux, it traverses the ocean from north to south, producing a freshwater flux in the same direction as the salt flux.

Considering these two facts it turns out that an accurate estimate of the transport through Bering Strait is very important for the correct determination of both the salt and freshwater fluxes. In the discussion of the Arctic Mediterranean Sea (Chapter 7) we argued that mass transport through Bering Strait is less than 1 Sv and can be neglected in the global mass budget; in other words, in any model of the global oceanic circulation Bering Strait could

south Atlantic Ocean to zero in the Arctic Mediterranean Sea. Wijffels *et al*. (1991) pointed out only recently that the surface salinities of the north Pacific Ocean are so low (near 32, see Figure 2.5b) that their freshwater content relative to the global mean salinity is of order 10%. In their budget calculations they use 1.5 Sv for the flow through Bering Strait; this produces a freshwater transport of 150,000 m^3 s^{-1}, several times the mean flow of the Amazon River! Thus the Bering Strait throughflow is a major contributor to the world freshwater balance, and if it is accounted for, freshwater transport in the Atlantic Ocean is southward everywhere. Figure 18.5 shows the resulting global flux distribution for salt and freshwater. Note that unlike freshwater, salt does not escape through the sea surface, so the salt transport is the same in each of the major subdivisions of the world ocean.

This discussion illustrates why the north Pacific becomes so much fresher than the north Atlantic Ocean. One can imagine that if the two basins were suddenly forced to have equal salinities, Deep Water might form in both; but to maintain this state of affairs it would be necessary to increase the Central American land barrier sufficiently in order to suppress the flux of moisture from the Atlantic to the Pacific Ocean. With the present topography of Central America and rainfall distribution the surface salinity of the north Atlantic Ocean would gradually increase, while the surface salinity of the north Pacific Ocean would decrease, enhancing Deep Water formation in the Atlantic and retarding it in the Pacific Ocean. Pacific Deep Water formation would eventually cease, and near-surface salinities would continue to decrease in the north Pacific Ocean until they became so low that the small Bering Strait throughflow could drain off a freshwater flux equal to the flux over Central America. It is interesting to speculate what the surface salinity in the north Pacific Ocean must have been during the last Ice Age, when the Bering Strait was blocked.

Model heat flux patterns in the Southern Ocean

The discussion of the last few paragraphs carried us to the limits of what we can achieve with today's data set. Global budgets require global data coverage, which is difficult to achieve even with modern means. Satellites will make a major contribution here, at least for the global heat budget. But we are still desperately short of data particularly in the Southern Ocean (which is a major unknown in Figure 18.5). Recourse to numerical modelling is therefore essential if we want to learn more about the climate without waiting for many more years until the needed data arrive.

Numerical models of the oceanic circulation have the advantage that they do not depend on the details of the heat and evaporation algorithms used in generating Figs. 1.6 and 1.7; their estimates of the net surface heat flux depend only on the velocity, temperature and salinity fields of the model itself. Furthermore, most models force surface temperature and salinity (the best known observational parameters) to stay close to observed patterns. Their usefulness for predicting heat and freshwater fluxes therefore depends mainly on their skill in getting the ocean currents correct. In this section we will compare the surface heat flux field from one such model with the observations of Figures 1.6 and 1.7. The model heat flux field turns out to be in reasonable agreement with observations, over the region where data are adequate; similar results are found in a number of other ocean models. Hence it is reasonable to use such models to give us some ideas on the heat flux pattern in the Southern Ocean, where data are not adequate.

Figure 18.6 shows the model's equilibrium heat flux distribution for the world ocean. The observed heat flux pattern (Figure1.6) is generally reproduced by the model. The heat flux at the eastern Pacific and Atlantic boundaries is not as large as in the observations, but the model ocean gains heat near the coast from at least 40°S to 50°N in the Pacific, and from the Cape of Good Hope to Spain in the Atlantic Ocean. By contrast, heat is lost from the model ocean off western Australia south of 20°S, again in agreement with observations. No heat flux maximum is found in Indonesia because no allowance was made for enhanced vertical mixing in this region. As the model is driven only by annual mean wind stresses, the model heat flux in the western Indian Ocean comes out somewhat smaller than the observed annual mean. Strong heat fluxes out of the ocean occur in the Kuroshio and the Gulf Stream, and weak heat fluxes out of the ocean occur in the Brazil Current and the East Australian Current. All these features are qualitatively much the same as in the observations. Since the forcing of this model contains no seasonal cycle, its broad agreement with reality provides one reason for believing that much of the net heat flux into the ocean is controlled by the annual mean currents.

The similarities between model and observations encourage us to tentatively interpret the model heat fluxes in data-poor regions, as if they were real. It is worth examining the nature of the model surface heat budget in some detail for the Southern Ocean, because the results of this and other models provide the most reliable guide so far as to the nature of heat exchange processes in this very important part of the ocean.

It is evident from Figure 18.6 that two large bands of heat loss from the ocean occur in the model Southern Ocean, stretching eastward and slightly southward from the Agulhas retroflection and from New Zealand. This tends to confirm the suspicion that the observations must be missing a large part of the heat loss from the Agulhas and East Australian Current systems, respectively. Support for the value of the model also comes from the fact that the two heat loss bands coincide with observed locations of Subantarctic Mode Water formation (Chapter 6). Heat loss leads to convective overturn, and the model, too, shows deep mixed layers beneath the heat loss bands.

Two distinct bands of oceanic heat gain are seen south of the two heat loss bands. One occurs in the Atlantic and western Indian Ocean, south of the Agulhas Current; the second occurs south of the New Zealand boundary current. In these regions Ekman transports are northward and increase northwards, so that upwelling occurs, and surface water is moved towards warmer climates; both processes will favour heat gain by the ocean. Further south still more heat loss occurs near the Antarctic continent, associated with bottom water formation in the model. However, since the model does not allow for sea ice formation the details cannot be expected to be very realistic.

The model just discussed represents the ocean through a network (or "grid") of data points of between 200 km and 300 km separation. It is therefore unable to resolve the quasigeostrophic eddies which are so ubiquitous in the ocean and in some regions (particularly in the Southern Ocean; see Chapter 6) essential for the transport of heat and salt. Other models which use the most powerful computers presently available use grid representations with mesh sizes as small as 15 km. While we cannot expect these models to reproduce actually observed eddies in size, location, or life span, we can hope that the models reproduce the eddy statistics such as the distribution of eddy kinetic energy (Figure 17.10) and improve our estimates of oceanic heat flux by identifying the relative importance of eddy heat transport in different regions of the world ocean.
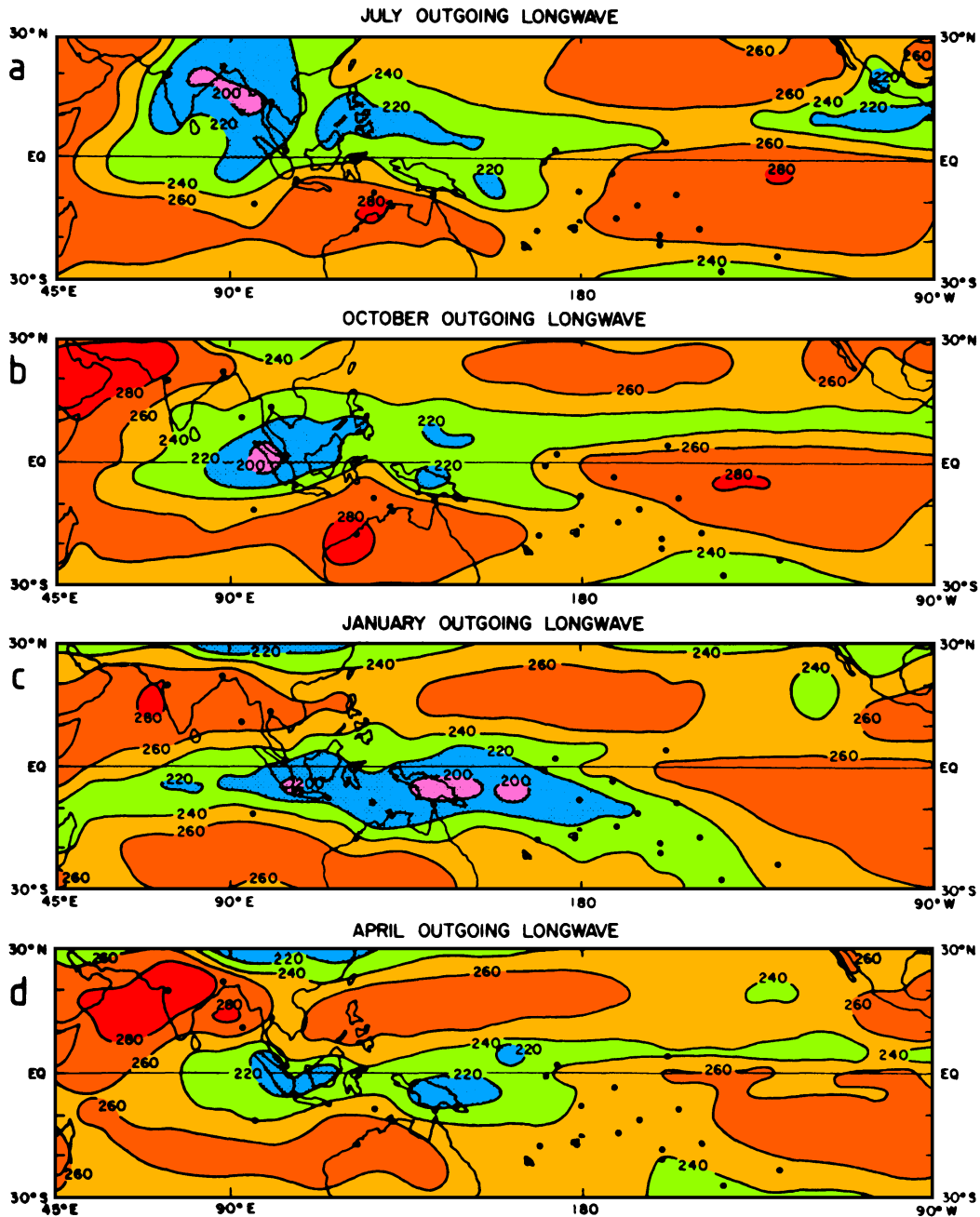
JULY OUTGOING LONGWAVE

a

OCTOBER OUTGOING LONGWAVE

b

JANUARY OUTGOING LONGWAVE

c

APRIL OUTGOING LONGWAVE

d

Fig.18.7. Long-term mean of outgoing longwave radiation (OLR, W m^{-2}) for the period June 1974 - November 1983 but excluding 1978, for the Indian and Pacific sectors. (a) July, (b) October, (c) January, (d) April. Areas of less than 220 W m^{-2} OLR are stippled, indicating greatest tropical convection. Adapted from Janowiak *et al*. (1985).